Theoretical Study of Phase Transition, Surface Tension, and Nucleation Rate Predictions for Argon

4 AUTHORS, INCLUDING:

Di Zhou
Qufu Normal University
5 PUBLICATIONS   **31** CITATIONS

SEE PROFILE

Jianguo Mi
Beijing University of Chemical Technology
75 PUBLICATIONS   **534** CITATIONS

SEE PROFILE

Theoretical Study of Phase Transition, Surface Tension, and Nucleation Rate Predictions for Argon

Di Zhou, Ming Zeng, Jianguo Mi,* and Chongli Zhong

Laboratory of Computational Chemistry, Department of Chemical Engineering, Beijing University of Chemical Technology, Beijing 100029, China

In this work, a weighted density functional theory has been used to study the equilibrium and metastable processes for argon. In the theoretical approach, the two- and three-body interactions of the fluid molecules are considered simultaneously, and the renormalization group transformation is applied to address the long-range fluctuations inside the critical region. The global phase equilibria, planar and curvature-dependent surface tensions, critical radius, and nucleation rates of argon are investigated systematically. The results are in good agreement with the experimental data. Meanwhile, this work applies a methodology for calculating the curved surface tension in local supersaturated environments, showing that the Tolman length is negligible far from the critical region. Near the critical point, however, the Tolman length becomes positive and appears to diverge.

1. Introduction

Knowledge of the nucleation mechanism in condensation of supersaturated vapors is of special significance in many scientific fields and numerous technical applications.[1−3] In the process of first-order phase transitions, gas molecules begin to aggregate and form nuclei under the environment of supersaturation. Small clusters have to reach a critical size located at the top of the free energy barrier before they can serve as nuclei of the new phase. These nuclei determine the rate at which droplets form as a function of the degree of supersaturation and have been well documented.[4−6] However, the question of how the phase transition proceeds on the molecular scale and the magnitude of the nucleation rate are still far from fully clarified.

In numerous homogeneous nucleation systems, argon plays an exceptional role for theory, simulation, and experiment studies because of its relatively simple structure and properties. Recently, new experimental techniques have been designed to carry out argon nucleation experiments.[7−11] The nucleation rate[7−11] was measured in the cryogenic environments with helium as the carrier gas. Nevertheless, an accurate experimental measurement is still difficult: a homogeneous system without walls or other irregularities should be closely approximated; the accessible range of the nucleation rate is limited to comparatively slow processes that are relatively far from the spinodal.

Molecular simulation provides an important source of information on nucleation in simple fluids. In molecular simulation, homogeneous nucleation can be studied either by direct observation or by indirect derivation from the size of the critical nucleus and Gibbs energy of formation. In recent years, the planar and curvature-dependent interfacial tensions, critical nucleus sizes, and nucleation rates of the Lennard-Jones (LJ) fluid have been extensively investigated by Monte Carlo (MC)[12−16] and molecular dynamics (MD)[17−21] simulations. Although great progress has been achieved, these works still show obvious discrepancies with respect to the experimental results. There are many factors that can be behind such discrepancies. One important issue is that the calculated properties of argon (especially vapor pressure and surface tension) in the simulations are far from that of experiments.[22] During simulations, the truncation of intermolecular interactions due to the finite size of simulation box is inevitable, and the long-range correlation or tail correlation has to be considered. This kind of correlation has been well discussed.[22−24]

Theoretical models provide an alternative way to describe droplet nucleation. In recent years, the spectrum of theoretical models of nucleation has been significantly broadened. The oldest and most widespread approach is the classical nucleation theory (CNT), which was developed by Becker and Döring.[25] The advantage of the theoretical models lies in predicting the free energy barrier and the critical cluster size in terms of macroscopic properties that are accessible by experiments, including the liquid density and the surface tension. However, it assumes that the cluster behaves as an infinite bulk liquid phase with regard to density and surface tension, which appears to contradict the fact that clusters are finite objects. It can underestimate the nucleation rate for argon up to 26 orders of magnitude deviation from experiment.[26] Later, various approaches were proposed to calculate the free energy of clusters of arbitrary size, such as the dynamic nucleation theory (DNT)[27−29] and the mean-field kinetic nucleation theory (MKNT).[30] It was shown that the DNT yields similar accuracy as CNT, and the MKNT is slightly better than the DNT in predicting the experimental data. Therefore, these theoretical models seem to be unable to describe the nucleation process for argon quantitatively.

Compared with the above theoretical models, the minimum free energy route offers advantages in understanding the nucleation mechanism. In this regard, density functional theory (DFT) provides a promising way to extract information about the interfacial free energy. In recent years, a number of beneficial attempts have been made to improve the density functional approach, such as the modified-core van der Waals model[31] and the introduction of time integration of the phase-field equation.[32]

In this work, we develop a density functional method to study the growth of the model argon droplets from the supersaturated vapor. Because the growing cluster is in a nonequilibrium state characterized by the given variables, the present theory departs from the traditional concept by recognizing that the gas phase

---

* Corresponding author. E-mail: mijg@mail.buct.edu.cn.

58 *J. Phys. Chem. B, Vol. 115, No. 1, 2011*

Zhou et al.

is also in a nonequilibrium state, with the vapor pressure immediately above the surface of the droplet being determined by the fast diffusion across the interface rather than the slower diffusion into the bulk gas reservoir.[33] Unlike the CNT, in which the planar vapor−liquid interfacial tension is the crucial input, a novel curvature effect on the excess free energy of the liquid droplets has been taken fully into account that is distinct from the essentially geometrical contributions from the Tolman length.[33,34] In our previous works,[35,36] it was shown that the combination of the modified fundamental measurement theory (MFMT)[37] with the first-order mean spherical approximation (FMSA)[38,39] yields more accurate results than those from the classical density functional model[40] in prediction of bulk and vapor−liquid interfacial properties of fluids. In the present model, the well-addressed MFMT is adopted to describe the hard sphere reference term. For the attractive part, the free energy is constructed by combining that of the bulk fluid with weighted density approximation. More importantly, both the two- and the three-body interactions of argon molecules are considered, and the long-range density fluctuation inside the critical region has been also included by the renormalization group (RG) transformation. With the new method, the vapor−liquid phase equilibria and the planar interfacial tensions are calculated with the same parameters to reproduce the experimental values. By expanding the surface tension of a cluster in powers of its curvature, the magnitude of the Tolman length as a function of temperature and the Tolman correlation are analyzed. Finally, the critical nucleus size and nucleation rate of the model argon are predicted based on the improved free energy barrier calculation. To test our model, we compare all the calculated results with the relevant simulation and experimental data.

2. Theory

To improve the accuracy of the free energy calculation, we consider the two- and three-body interactions of molecules simultaneously. The applied potential in this work can be written as the sum of the pair and triplet potentials

$$u(r) = \varphi_2(r) + \varphi_3(r) \qquad (1)$$

where $\varphi_2(r)$ represents the pair potential and $\varphi_3(r)$ represents the triplet potential[41] and can be given by

$$\varphi_2(r) = 4\varepsilon\left[\left(\frac{\sigma}{r}\right)^{12} - \left(\frac{\sigma}{r}\right)^6\right] \qquad (2)$$

and

$$\varphi_3(r_1, r_2, r_3) = \frac{\nu(1 + 3\cos\theta_1\cos\theta_2\cos\theta_3)}{(r_1 r_2 r_3)^3} \qquad (3)$$

respectively. Here ε is the energy parameter, σ is the soft diameter. r_1, r_2, r_3, θ_1, θ_2, and θ_3 are the sides and interior angles of the triangle formed by the molecules 1, 2, 3, and ν is the three-body interaction coefficient, which is known to be 73.2 × 10^{-84} erg·cm[9] for argon.

Perturbation with RG Transform for Vapor−Liquid Equilibria. The reduced Helmholtz free energy density for argon in bulk fluid is usually expressed as a summation of the

ideal, hard sphere repulsion, and the dispersion attraction contributions

$$f = \rho[\ln(\rho\Lambda^3) - 1] + f^{\text{hs}} + f^{\text{att}} \qquad (4)$$

in which Λ is the de Broglie wavelength and ρ is the density of bulk fluid. The hard sphere contribution is given by

$$f^{\text{hs}} = \rho\frac{4\eta - 3\eta^2}{(1 - \eta)^2} \qquad (5)$$

Here $\eta = (1/6)\pi\rho d^3$ is the packing factor, with d given by the Barker−Henderson perturbation theory[42]

$$d = \frac{1 + 0.2977T^*}{1 + 0.33163T^* + 0.00104771T^{*2}}\sigma, \ T^* = \frac{k_{\text{B}}T}{\varepsilon} \qquad (6)$$

where k_{B} is the Boltzmann constant. According to Lee and Barker,[41] the dispersion contribution is given by a sum of perturbation terms

$$f_{\text{att}} = f_1 + f_2 \qquad (7)$$

$$f_1 = 2\pi\rho \int_\sigma^\infty g(r)\varphi_2(r)r^2 \, dr \qquad (8)$$

$$f_2 = \frac{\rho^2}{6} \int_V \int_V \varphi_3(r_1, r_2, r_3)g(r_1)g(r_2)g(r_3) \, d\mathbf{r_2} \, d\mathbf{r_3} \qquad (9)$$

where V is a macroscopic volume and $g(r)$ is the radial distribution function (RDF) for pair potential and can be given by the FMSA[38,43] with the simplified exponential approximation

$$g(r) = g_0(r) \exp[g_1(r)] \qquad (10)$$

and

$$rg_0(r) = \sum_{n=0}^\infty (-12\eta)^n C(1, n+1, n+1, r-n-1) \qquad (11)$$

$$\begin{aligned} rg_1(r) = {}&\beta\varepsilon k_1\frac{(1-\eta)^4}{Q^2(z_1)}\sum_{n=0}^\infty (1+n)(-12\eta)^n \times \\ &D(6, n, n+2, z_1, r-n-1) \\ -{}&\beta\varepsilon k_2\frac{(1-\eta)^4}{Q^2(z_2)}\sum_{n=0}^\infty (1+n)(-12\eta)^n \times \\ &D(6, n, n+2, z_2, r-n-1) \end{aligned} \qquad (12)$$

where $C(n_1, n_2, n_3, r)$ and $D(n_1, n_2, n_3, z, r)$ are defined elsewhere.[43]

With eq 4, the phase coexistence curves can be calculated directly. Therefore, obtained results are reasonable outside the critical region. Inside the critical region, the deviations caused by the long-range density fluctuation can be remedied with the RG transformation[44,45]

Predictions for Argon

J. Phys. Chem. B, Vol. 115, No. 1, 2011 **59**

$$f_n(\rho) = f_{n-1}(\rho) + \Delta f_{RG,n}(\rho) \qquad (13)$$

$$\Delta f_{RG,n}(\rho) = -\frac{1}{\beta V_n} \times$$

$$\ln \left[\frac{\int_0^\rho dx \exp\{-V_n[\beta f_{n-1,D}(\rho, x) + 2\pi C_4 x^2 k_n^2 - 2\pi C_6 x^2 k_n^4]\}}{\int_0^\rho dx \exp\{-V_n[\beta f_{n-1,D}(\rho, x) + 2\pi C_2 x^2]\}} \right] \qquad (14)$$

$$f_{n-1,D}(\rho, x) = \frac{f_{n-1}(\rho + x) + f_{n-1}(\rho - x)}{2} - f_{n-1}(\rho) \qquad (15)$$

$$C_n(r) = \frac{1}{(n-1)!} \int_0^\infty c(r) r^n \, dr \qquad (16)$$

where V_n is the phase space volume of n-order RG iterations $V_n = \lambda_n^3$, with $\lambda_n = 3^{n-1}\lambda_1$ and $\lambda_1 = 4\sigma$, k_n is the fluctuation magnitude $k_n = k_1/3^{n-1}$ with $k_1 = 2\pi/\lambda_1$, and $c(r)$ is the direct correlation function (DCF), defined in ref 35. The initial f_0 can be calculated by eq 4. After several iterations, the free energy due to long-range density fluctuation can be incorporated into the short-range contribution.

Planar and Curvature-Dependent Surface Tensions. The density distribution of the vapor–liquid interface can be given by minimizing the grand potential and solving the Euler–Lagrange equation

$$\rho(\mathbf{r}) = \rho_b \exp\left(\beta\mu - \beta\frac{\partial(F_{hs}[\rho(\mathbf{r})] + F_{att}[\rho(\mathbf{r})])}{\partial\rho(\mathbf{r})} - \beta\frac{\partial[\Delta F_{RG}(\rho_{av})]}{\partial\rho_{av}}\right) \qquad (17)$$

where ρ_b means the bulk density, μ indicates the chemical potential of the bulk fluid, $\rho(\mathbf{r})$ denotes the density distribution at the distance $\mathbf{r}$, $F_{hs}[\rho(\mathbf{r})]$ stands for the local Helmholtz free energy of hard-sphere reference system, which can be given by the MFMT,[36] $F_{att}[\rho(\mathbf{r})]$ represents the local Helmholtz free energy of the attractive contribution, and $\Delta F_{RG}(\rho_{av})$ expresses the Helmholtz free energy due to the long-range density fluctuation. Because the long-range fluctuation is conducted on the bulk density, ρ_{av} is the average density of the inhomogeneous fluid with $\rho_{av} = (\rho_l + \rho_v)/2$.

According to the MFMT, the hard-sphere repulsive contribution for the density functional can be represented by

$$\frac{\partial\beta F_{hs}[\rho(\mathbf{r})]}{\partial\rho(\mathbf{r})} = \sum_\alpha \int \frac{\partial\phi_{hs}}{\partial n_\alpha} w^{(\alpha)}(\mathbf{r} - \mathbf{r}') \, d\mathbf{r}' \qquad (18)$$

$$\phi_{hs} = -n_0 \ln(1 - n_3) + \frac{n_1 n_2 - \mathbf{n_{V1} n_{V2}}}{1 - n_3} +$$

$$\frac{1}{36\pi}\left(n_3 \ln(1 - n_3) + \frac{n_3^2}{(1-n_3)^2}\right)\frac{n_2^3 - 3n_2 \mathbf{n_{V2} n_{V2}}}{n_3^3} \qquad (19)$$

where $w^{(\alpha)}(r), \alpha = 0,1,2,3,\mathbf{V1},\mathbf{V2}$ are the scalar and vector weight functions and $n_\alpha(r)$ is the weighted density. They are given by the fundamental measure theory.[46]

For the attractive part, we introduce the hybrid weighted-density approximation, which was proposed by Leidl and Wagner.[47] In this case, the partial derivative of the free energy functional is written as

$$\frac{\partial\beta F_{att}[\rho(\mathbf{r})]}{\partial\rho(\mathbf{r})} = \beta\frac{f_{att}[\bar{\rho}(\mathbf{r})]}{\bar{\rho}(\mathbf{r})} + \beta\int\rho(\mathbf{r}')\frac{\partial(f_{att}[\bar{\rho}(\mathbf{r}')]/\bar{\rho}(\mathbf{r}'))}{\partial\bar{\rho}(\mathbf{r}')} \times \omega_{att}(|\mathbf{r} - \mathbf{r}'|) \, d\mathbf{r}' \qquad (20)$$

with

$$\bar{\rho}(\mathbf{r}) = \int\rho(\mathbf{r}')\omega_{att}(|\mathbf{r} - \mathbf{r}'|) \, d\mathbf{r}' \qquad (21)$$

in which $\omega_{att}(r)$ is another weight function, and $f_{att}[\bar{\rho}(r)]$ is given by eq 7. According to Denton and Ashcroft,[48] we assume that the weighted function $\omega_{att}(r)$ can be determined by the attractive part of DCF with an approximation

$$\omega_{att}(r) = \frac{c_{att}(r)}{\int c_{att}(r) \, d\mathbf{r}} \qquad (22)$$

It is acceptable to use only the two-body DCF to get $\omega_{att}(r)$ because $\omega_{att}(r)$ is only a weight function that has no influence on the three-body free energy f_2, which is a part of $f_{att}[\bar{\rho}(r)]$ included in eq 20. Because $c_{att}(r)$ inside the molecular is dependent on the bulk density,[35] if it is used to construct the weight function, then it would deteriorate the thermodynamic consistency of the model.[49] In this regard, it can be modified as $c_{att}(r) = -\varepsilon$ within $r < \sigma$.

To obtain the interfacial density profile, eq 17 can be calculated using the Picard iteration. The iteration terminates when the maximum difference between two subsequent density profiles is $<10^{-6}$. Therefore, the constrained free energy for the vapor–liquid interface or liquid droplet can be expressed as

$$\Delta\Omega = \int d\mathbf{r} \, \rho(\mathbf{r})[\ln(\rho(\mathbf{r})\Lambda^3) - 1] + F_{rep}[\rho(\mathbf{r})] + F_{att}[\rho(\mathbf{r})] + \Delta F_{RG}(\rho_{av}) + pV \qquad (23)$$

where p is the pressure. For the planar interface, p represents the saturation vapor pressure p^+, where the superscript denotes the equilibrium state, and in the following it stands for the same meaning; whereas for a nucleating droplet, it is the vapor pressure above the surface of the liquid. Equation 23 is fundamental for the planar and curved surface to calculate the surface tension and the free energy barrier of nucleation. The planar and curvature-dependent surface tensions can be calculated by

$$\gamma^+ = \frac{\Delta\Omega}{A} = \int_0^\infty [f[\rho(z)] - \rho(z)\mu + p] \, dz \qquad (24)$$

and

$$\gamma = \frac{\Delta\Omega + 4/3\pi R^3 \Delta p}{4\pi R^2} = \int_0^\infty \left(\frac{r}{R}\right)^2 [f[\rho(r)] - \rho(r)\mu + p] \, dr + \frac{1}{3}R\Delta p \qquad (25)$$

60 *J. Phys. Chem. B, Vol. 115, No. 1, 2011*

Zhou et al.

respectively. In eqs 24 and 25, A is the interfacial surface area, $f[\rho(r)]$ is the excess Helmholtz free energy density with $F[\rho(\mathbf{r})] = \int d\mathbf{r}\, f[\rho(\mathbf{r})]$, Δp is the pressure difference between the droplet and the supersaturated vapor, and R is the radius of droplet. The details of R and Δp will be discussed below. Subsequently, the Tolman length δ can be estimated by fitting γ in terms of the Helfrich formula[50] with the second-order expansion

$$\gamma = \gamma^+ - \frac{2\delta\gamma}{R} + \frac{k_s}{R^2} \qquad (26)$$

Here k_s is the rigidity coefficient.

Critical Nucleus Size and Nucleation Rate. In the process of nucleation, the extremum of the constrained free energy of a single growing droplet is a saddle point. The mechanical equilibrium is manifest in the Laplace equation

$$\Delta p = \frac{2\gamma}{R} \qquad (27)$$

where $\Delta p = p_l - p_v$ and p_l and p_v are the pressure in the liquid and vapor region, respectively. The pressure p_l in the droplet is that of a hypothetical bulk liquid phase, which has a chemical potential $\mu_l(p_l,T)$ equal to the chemical potential $\mu_v^{local}(p_v,T)$ of the local supersaturation vapor. Following Moody,[33] we assume the vapor pressure above the droplet surface p_v^{local} is different from the pressure of bulk vapor p_v. And the corresponding local supersaturation ratio is $S^{local} = p_v^{local}/p^+$. S^{local} varies with the size of the droplet. The stationary condition is $\mu_l = \mu_v^{local}$, which, with the ideal gas and incompressible liquid assumption, gives

$$p_l = p^+ + k_B T \rho_l \ln S^{local} \qquad (28)$$

where ρ_l is the density of droplet.

Substituting eq 28 into eq 27, the radius of droplet R as a function of the local supersaturation ratio S^{local} can be obtained by

$$S^{local} - 1 + 2\gamma/Rp^+ - (k_B T\rho_l/p^+)\ln S^{local} = 0 \qquad (29)$$

The constrained free energy of the droplet with radius R can also be given by

$$\Delta\Omega = -\frac{4}{3}\pi R^3 \Delta p + 4\pi R^2 \gamma \qquad (30)$$

The energy of a growing droplet can be calculated through eqs 17 and 23. As the free energy barrier of the droplet formation reaches a maximum, the size of droplet is defined as the critical radius, and the local supersaturation S^{local} is equal to the supersaturation ratio of the bulk vapor S. Substituting eqs 27 and 30 into eq 23, we can obtain the accurate critical nucleation radius

$$R = (3\Delta\Omega/2\pi\Delta p)^{1/3} \qquad (31)$$

The corresponding nucleation rate is

$$J = K \exp\left(\frac{-\Delta\Omega}{k_B T}\right) \qquad (32)$$

where the kinetic prefactor reads

$$K = \frac{(\rho_v)^2}{\rho_l}\sqrt{\frac{2\gamma(R)}{\pi m_l}} \qquad (33)$$

Here m_l is the mass of a molecule and ρ_l and ρ_v are the densities of droplet and supersaturated vapor, respectively.

3. Results and Discussion

In the following discussions, we define the above-described approach as the full model to compare with a simplified model, in which only the three-body contribution of the full model is omitted. The simplified model is used to test the full model. We have calculated phase equilibria, surface tension, critical radius, and nucleation data by the two models. Representative results are presented and compared with those simulation or experimental data. Because the molecular parameters of argon are the best fit to the experimental vapor−liquid equilibria data, the values for the simplified and full models are slightly different. Given by the molecular simulations,[24,41] for the simplified model, the diameter σ is 3.40 Å, and the energy parameter ε/k_B is 119.4 K; whereas for the full model, σ is 3.3605 Å and ε/k_B is 119.4 K.

Global Vapor−Liquid Phase Diagram. We first calculate the global vapor−liquid phase behavior of argon by the simplified and full model, respectively. The calculated results and the experimental data[51] are shown in Figure 1. Far from the critical region, the two models produce nearly the same results as the experimental data. These good results are due to the best fitting molecular parameters. Near the critical region, the results given by the simplified model deviate systematically by overestimating the phase coexistent curves. If the three-body interactions are included, then the full model performs much better. With further modification with the RG transformation, the full model can reproduce the experimental results throughout the global vapor−liquid phase diagram. In particular, the calculated critical temperature T_C is 152.7 K, the critical density ρ_C is 13.73 mol/L, and the critical pressure P_C is 5.45 MPa. Compared with the experimental data (150.7 K, 13.41 mol/L, 4.86 MPa),[51] the calculated critical temperature and density are quite accurate, whereas the calculated critical pressure is higher. Figure 1 also indicates that even without the RG transformation the theory that incorporates triplet interactions yields quite good results inside the critical region, and the largest predictive error is no more than 5% for temperature, density, or pressure, respectively. The calculation error is acceptable for engineering application.

Vapor−Liquid Interfacial Tension. Figure 2 shows the planar surface tensions as a function of temperature. One can find that the results given by the simplified model are similar to those of the simulation,[24] in which only two-body interactions are considered. The two curves show only a qualitative agreement with experimental observation of argon.[51] The average relative deviation is ∼20%, whereas for the full model the results are in good agreement with the experimental data. The surface tension vanishes as the critical temperature is approached. If the two- and three-body contribution are considered in the simulation,[41] then the good results are also
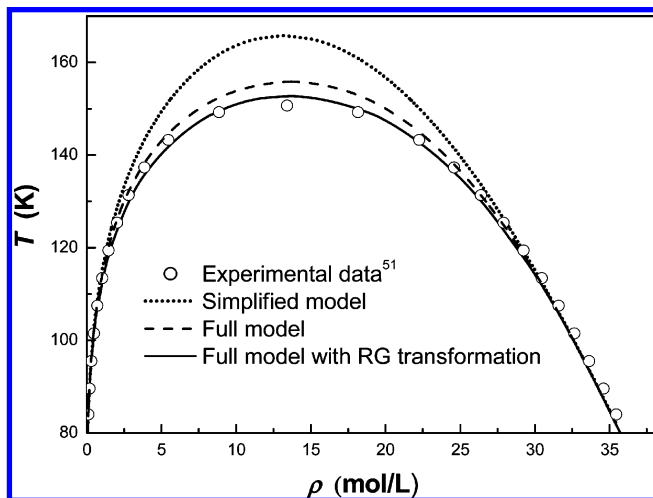
Predictions for Argon

J. Phys. Chem. B, Vol. 115, No. 1, 2011 **61**

Figure 1. Global vapor−liquid phase equilibria of argon.
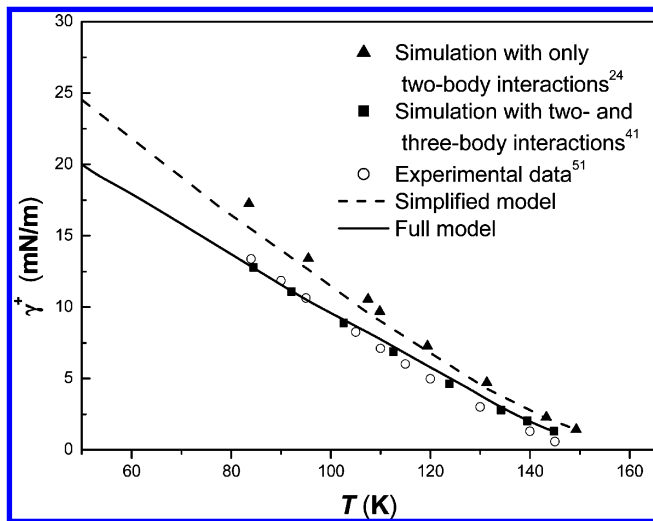
Figure 2. Vapor−liquid interfacial tension as a function of temperature.

Figure 3. Determination of the critical exponent, μ. The symbols are calculated results, and the solid lines are the best linear regression of the symbols.

Figure 4. Constrained Helmholtz free energy of a growing droplet at $T = 0.8\varepsilon/k_B$ and $S = 2$.

obtained. Figure 2 illustrates clearly that the three-body contribution is very important in the description of the surface tension.

Figure 3 shows the interfacial tensions given by the full model plotted against the temperature distance to the critical point. A fit to the scaling law is shown as the solid line. It gives a value for the critical scaling exponent of $\mu = 1.20$, closing to the universal exponent 1.26. The results indicate that the full model is reliable to predict the surface tension over a wide temperature range.

Curvature-Dependent Surface Tension and Tolman Length. A liquid droplet is thermodynamically unstable if it is surrounded by a local supersaturated vapor phase. In this case, the coexistence of the unstable liquid droplet with its surrounding vapor reflects a free energy variation, as shown in Figure 4, with the constant bulk supersaturation ($S = 2$). For the free energy calculation, R at different values is given. Each value of R corresponds to a local supersaturation ratio $S^{\text{local}} \equiv p_v^{\text{local}}/p^+$, as mentioned above. When $S^{\text{local}} = S$, the free energy curve achieves the maximum corresponding to the critical radius. Figure 4 also compares the free energy variation in the droplet nucleation process given by the simplified and full models that take into account the effect of supersaturation with the results given by the CNT and the molecular simulation. It is shown that the calculated maximum free energy barrier of nucleation and the critical radius by the full model are quite in agreement
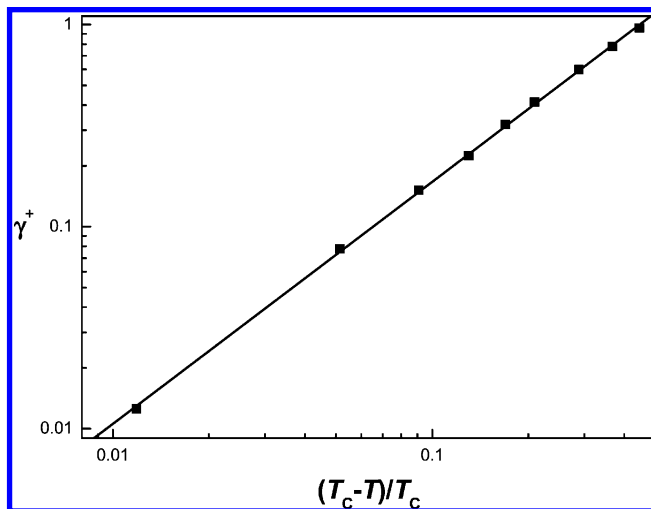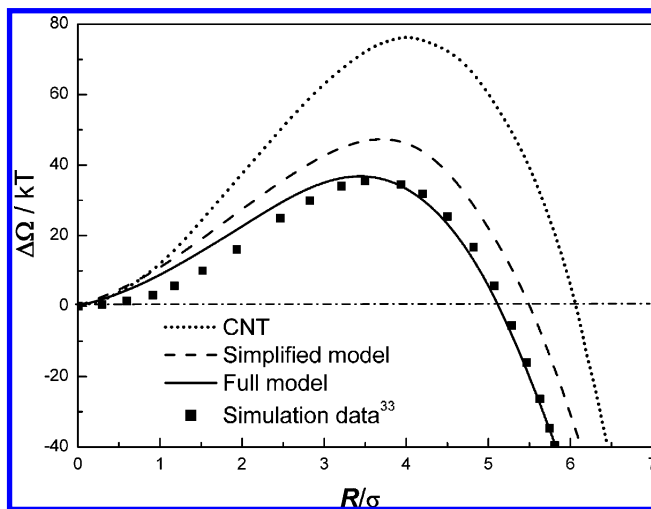
with the simulation data,[33] whereas the simplified model overestimates the free energy barrier as well as the critical radius, and the CNT yields even more poor results.

The formation of a macroscopic liquid drop involves the stage of formation of nuclei of critical size. To calculate the properties of a prenucleation droplet, we follow the method originally proposed by Zeng and Oxtoby.[52] At a given temperature, the initial guesses of the densities for the liquid and vapor phases are obtained from the densities of the equilibrium liquid and that of the supersaturated vapor. The critical size of nuclei is obtained from eqs 27 and 30. Therefore, the curvature-dependent surface tensions are calculated under the condition of the critical radius R of the droplet at a given supersaturated environment. Figure 5 shows the relative surface tension given by the full model as a function of supersaturation ratio at different temperatures under the environment of $S^{\text{local}} = S$. Although the surface tension decreases with increasing supersaturation and vanishes approaching the planar limit asymptotically, the tendency of decline is different at different temperatures. At low temperature, the curvature-dependent surface tension show a slight decline, which means that a correlation of curvature on surface tensions is negligible at least under the low supersaturated environment, whereas at high temperature, the curves show a rapid decrease, and the corresponding correlation is necessary.
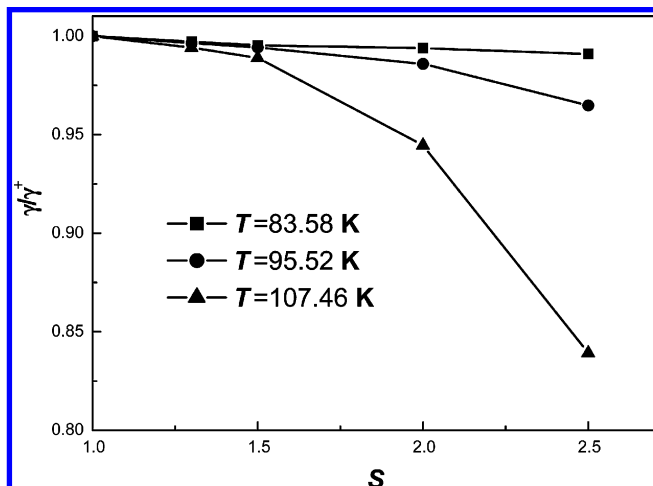
Figure 5. Curvature-dependent surface tension γ as a function of the supersaturation ratio at different temperatures when $S^{local} = S$. γ^+ is the planar coexistence surface tension.
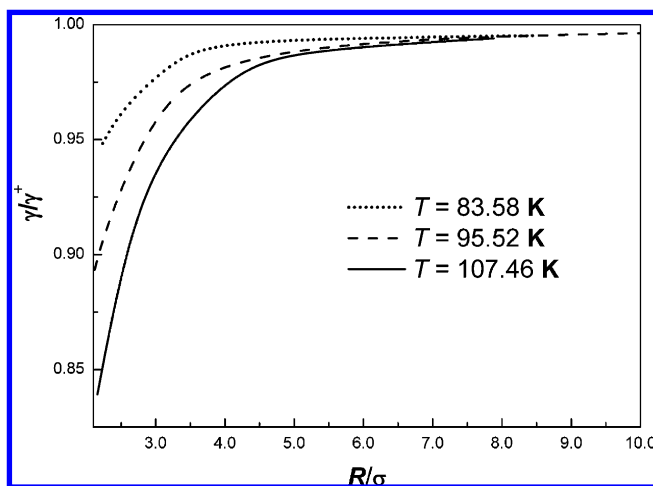

Figure 6. Relative surface tension as a function of critical droplet radius at different temperatures.

Figure 7. Regressed Tolman length as a function of temperature.

Figure 8. Experimental nucleation-rate $J_{exp} = 10^7$ cm^{-3} s^{-1} and the calculated isotherm as a function of supersaturation. The dashed and solid lines are results from the simplified and full model, respectively.

Meanwhile, the relative surface tensions as a function of the critical droplet radius are shown in Figure 6. For small droplets ($R = 2\sim6\sigma$), the relative surface tension increases rapidly as the radius grows, and the ratio is even obvious at low temperature. If the droplet radius is larger than 6σ, then the relative surface tension increases slowly to approach its planar value. Using eq 26, the Tolman length as a function of temperature is determined. The result is shown in Figure 7. Because the experimental values have not yet been determined, a qualitative analysis can be made to compare with the results by simulation. Far from the critical point, the Tolman length is negative and close to zero, which suggests that the first-order correction to the surface tension is insignificant. Our DFT calculations support the conjecture by Wolde and Frenkel, assuming that the Tolman length is zero.[12] Near the critical point, the Tolman length becomes positive and appears to diverge. The result is consistent with that of Giessen and Blokhuis[21] but is dissimilar to previous DFT predictions.[53] Although the molecular dynamics simulation[12,15] showed that the Tolman length is positive over a large temperature range, with magnitude typically on the order of a few tenths of the LJ molecular diameter, the prediction of the sign of the Tolman length based on computer simulation is still inconclusive to date. Because of the sensitivity of the Tolman length measurement on the form
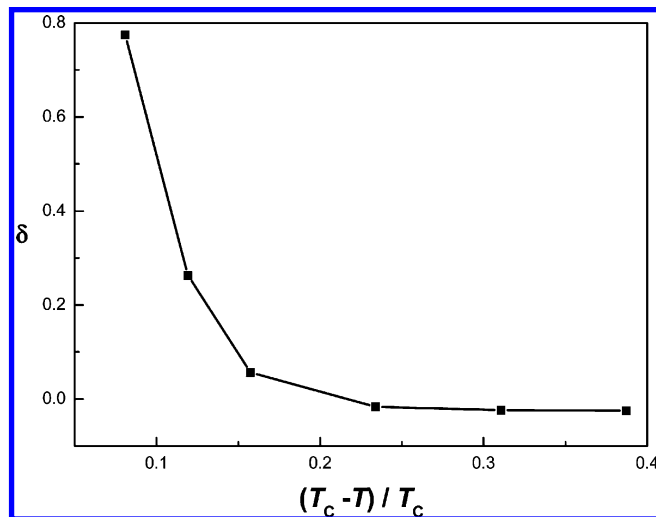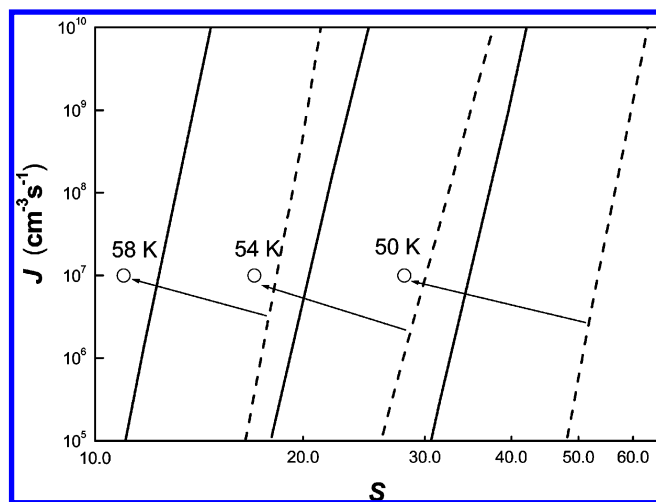
of the polynomial fit to the contact density, it indicates that the results can be taken as a guide to its size but not as an exact result.

Nucleation Rate. With the obtained energy barrier, the nucleation-rate isotherms as a function of supersaturation are computed using eq 32. The results given the simplified and full model are depicted in Figure 8. Open circles in the Figure correspond to the experimental data ($J_{exp} = 10^7$ cm^{-3} s^{-1}). According to Iland et al.,[8] the CNT yields 16−26 orders of magnitude difference when compared with experimental data, and a self-consistent theory of Girshick and Chiu[54] showed improved temperature dependence but still discrepancies of 11−17 orders of magnitude when compared with experimental data. The thermodynamically consistent theory of Kashchiev[55] predicted rates about 5−7 orders of magnitude below the experimental ones. In this work, we find that the predicted nucleation rates with respect to the temperature dependence are about two to three orders of magnitude below the experimental rates.[8] We cannot ensure that the calculated nucleation rate is in accordance with experimental nucleation rate over a wide range of temperature because such measurements have not been done yet. However, the present work shows that the full model is able to predict the characteristics of the nucleation rate quantitatively. In comparison, the calculated rates by the simplified model are about 10−13 orders of magnitude below
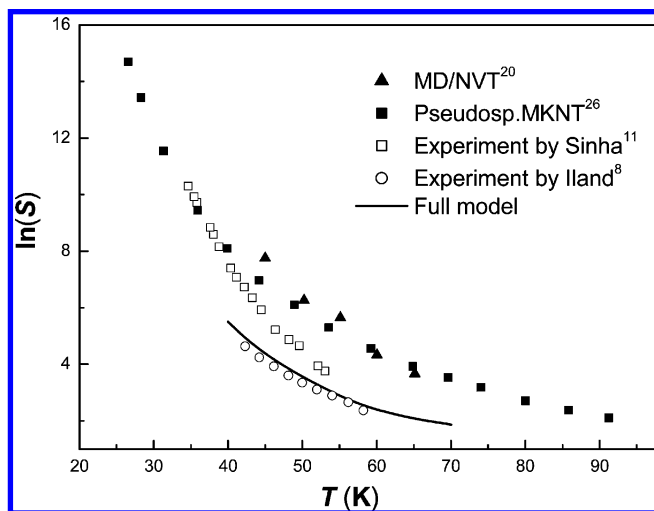
Predictions for Argon

J. Phys. Chem. B, Vol. 115, No. 1, 2011 **63**

Figure 9. Local supersaturation ratio of nucleation as a function of temperature given by the theoretical models, simulation, and experiments. The nucleation rate is constant to $J = 10^7$ cm^{-3} s^{-1}, except for the experiment[11] ($J = 10^{17}$ cm^{-3} s^{-1}).

the experimental data.[11] It is shows clearly that without consideration of the three-body interactions the present approach is not better than Kashchiev's method.

Figure 9 shows the supersaturation ratio as a function of temperature with the constant nucleation ratio ($J_{exp} = 10^7$ cm^{-3} s^{-1}). From the Figure, one can find that the results given by the full model are similar to the experimental data,[8] whereas the MKNT theory[26] and MD simulation[20] overestimate the degree of supersaturation from low to high temperature. Very recently, Sinha et al.[11] has measured pressures and temperatures under a different constant nucleation ratio ($J_{exp} = 10^{17}$ cm^{-3} s^{-1}). The results are also depicted in Figure 9 for comparison. This evidence indicates that the present model provides a good way for developing a theoretical model capable of describing the nucleation process.

4. Conclusions

In summary, a theoretical model has been developed to deal with the global vapor−liquid phase behavior, planar and curvature dependent surface tensions, and nucleation for argon. In the new model, an accurate weighted density functional method is employed, and the Helmholtz free energy due to the long-range density fluctuation inside the critical region is added by the RG transformation. Another important advantage is that the three-body interactions are taken into account. Compared with the experiment data, the model gives accurate global phase coexistence curves and vapor−liquid interfacial tensions both far from and near the critical point. With the curvature-dependent surface tensions, the Tolman length has been regressed. Far from the critical point, the Tolman length is negative and close to zero. As the temperature increases, it changes to positive. Near the critical region, a notable divergence appears. Similar phenomena was confirmed by a previous simulation but has not been previously discovered by a theoretical model. On the basis of an improved free energy barrier for nucleation, the model yields satisfactory nucleation rates for argon when compared with the recent experimental data. As a result, the new model provides a method not only to deal with the thermodynamic properties of argon in both bulk and inhomogeneous circumstances but also to obtain quantitative characteristics of the nucleation process.

References and Notes

(1) Abraham, F. F. *Homogeneous Nucleation Theory*; Academic: New York, 1974.
(2) Drossions, Y.; Kevrekidis, P. G. *Phys. Rev. E.* **2003**, *67*, 026127.
(3) Kashchiev, D. *Nucleation: Basic theory with Applications*; Butterworth-Heinemann: Oxford, U.K., 2000.
(4) Schrader, M.; Virnau, P.; Binder, K. *Phys. Rev. E.* **2009**, *79*, 061104.
(5) Carreón-Calderón, B.; Soria, A. *AIChE J.* **2009**, *55*, 2433.
(6) Li, Z.; Wu, J. *Ind. Eng. Chem. Res.* **2008**, *47*, 4988.
(7) Fladerer, A.; Strey, R. *J. Chem. Phys.* **2006**, *124*, 164710.
(8) Iland, K.; Wölk, J.; Strey, R.; Kashchiev, D. *J. Chem. Phys.* **2007**, *127*, 154506.
(9) Wedekind, J.; Hyvärinen, A. P.; Brus, D.; Reguera, D. *Phys. Rev. Lett.* **2008**, *101*, 125703.
(10) Wedekind, J.; Reguera, D.; Strey, R. *J. Chem. Phys.* **2007**, *127*, 064501.
(11) Sinha, S.; Bhabhe, A.; Laksmono, H.; Wölk, J.; Strey, R.; Wyslouzil, B. *J. Chem. Phys.* **2010**, *132*, 064304.
(12) Wolde, P. R.; Frenkel, D. *J. Chem. Phys.* **1998**, *109*, 9901.
(13) Punnathanam, S.; Corti, D. S. *Ind. Eng. Chem. Res.* **2002**, *41*, 1113.
(14) Shen, V. K.; Mountain, R. D.; Errington, J. R. *J. Phys. Chem. B.* **2007**, *111*, 6198.
(15) Neimark, A. V.; Vishnyakov, A. *J. Phys. Chem. B.* **2005**, *109*, 5962.
(16) He, S.; Attard, P. *Phys. Chem. Chem. Phys.* **2005**, *7*, 2928.
(17) Wang, Z.; Valeriani, C.; Frenkel, D. *J. Phys. Chem. B.* **2009**, *113*, 3776.
(18) Heyes, D. M. *Phys. Status Solidi B* **2008**, *245*, 530.
(19) Yasuoka, K.; Matsumoto, M. *J. Chem. Phys.* **1998**, *109*, 8451.
(20) Wedekind, J.; Wölk, J.; Reguera, D.; Strey, R. *J. Chem. Phys.* **2007**, *127*, 154515.
(21) Giessen, A. E.; Blokhuis, E. M. *J. Chem. Phys.* **2002**, *116*, 302.
(22) Moody, M. P.; Attard, P. *J. Chem. Phys.* **2001**, *115*, 8967.
(23) Mecke, M.; Winkelmann, J.; Fischer, J. *J. Chem. Phys.* **1997**, *107*, 9264.
(24) Janecek, J. *J. Phys. Chem. B.* **2006**, *110*, 6264.
(25) Becker, R.; Döring, W. *Ann. Phys.* **1935**, *24*, 719.
(26) Kalikmanov, V. I.; Wölk, J.; Kraska, T. *J. Chem. Phys.* **2008**, *128*, 124506.
(27) Schenter, G. K.; Kathmann, S. M.; Garrett, B. C. *Phys. Rev. Lett.* **1999**, *82*, 3484.
(28) Reguera, D.; Reiss, H. *Phys. Rev. Lett.* **2004**, *93*, 165701.
(29) Kathmann, S. M.; Schenter, G. K.; Garrett, B. C. *J. Chem. Phys.* **2002**, *116*, 5046.
(30) Kalikmanov, V. I. *J. Chem. Phys.* **2006**, *124*, 124505.
(31) Lutsko, J. F. *J. Chem. Phys.* **2008**, *128*, 184711.
(32) Tupper, P. F.; Grant, M. *Europhys. Lett.* **2008**, *81*, 40007.
(33) Moody, M. P.; Attard, P. *Phys. Rev. Lett.* **2003**, *91*, 056104.
(34) Bykov, T. V.; Zeng, X. *J. Chem. Phys.* **2006**, *125*, 144515.
(35) Tang, Y. *J. Chem. Phys.* **2004**, *121*, 10605.
(36) He, Y.; Mi, J.; Zhong, C. *J. Phys. Chem. B.* **2008**, *112*, 7251.
(37) Yu, Y.-X.; Wu, J. *J. Chem. Phys.* **2002**, *117*, 10156.
(38) Tang, Y.; Lu, B.C.-Y. *AIChE J.* **1997**, *43*, 2215.
(39) Tang, Y.; Wu, J. *Phys. Rev. E.* **2004**, *70*, 011201.
(40) Tarazona, P. *Phys. Rev. A.* **1985**, *31*, 2672.
(41) Lee, J. K.; Barker, J. A. *J. Chem. Phys.* **1974**, *60*, 1976.
(42) Barker, J. A.; Henderson, D. *J. Chem. Phys.* **1967**, *47*, 2856.
(43) Tang, Y.; Lu, B.C.-Y. *Mol. Phys.* **1997**, *90*, 215.
(44) Mi, J.; Zhong, C.; Li, Y.-G.; Tang, Y. *AIChE J.* **2006**, *52*, 342.
(45) Mi, J.; He, Y.; Zhong, C. *AIChE J.* **2009**, *55*, 747.
(46) Rosenfeld, Y. *Phys. Rev. Lett.* **1989**, *63*, 980.
(47) Leidl, R.; Wagner, H. *J. Chem. Phys.* **1993**, *98*, 4142.
(48) Denton, A. R.; Ashcroft, N. W. *Phys. Rev. A.* **1989**, *39*, 426.
(49) Sweatman, M. B. *Phys. Rev. E* **2001**, *65*, 011102.
(50) Blokhuis, E. M.; Bedeaux, D. *J. Chem. Phys.* **1992**, *97*, 3576.
(51) NIST Chemistry WebBook. http://webbook.nist.gov/chemistry (accessed 2010).
(52) Zeng, X.; Oxtoby, D. W. *J. Chem. Phys.* **1991**, *94*, 4472.
(53) Bykov, T. V.; Zeng, X. *J. Chem. Phys.* **2002**, *117*, 1851.
(54) Girshick, S. L.; Chiu, C. P. *J. Chem. Phys.* **1990**, *93*, 1273.
(55) Kashchiev, D. *J. Chem. Phys.* **2003**, *118*, 1837.

JP104969C